https://doi.org/10.5194/essd-2025-142
Preprint. Discussion started: 7 May 2025

Open Access Earth System Science Data Discussions

A high-quality daily nighttime light (HDNTL) dataset for global 600+ cities (2012-2024)

Zixuan Pei[1], Xiaolin Zhu[1,*], Yang Hu[2], Jin Chen[3], Xiaoyue Tan[1]

[1]Department of Land Surveying and Geo-Informatics, The Hong Kong Polytechnic University, Hong Kong, China
[2]Institute of Industrial Science, The University of Tokyo, Tokyo, Japan
[3]State Key Laboratory of Remote Sensing Science, Faculty of Geographical Science, Beijing Normal University, Beijing, 100875, China

**Correspondence to*: Xiaolin Zhu (xiaolin.zhu@polyu.edu.hk)

Abstract. Nighttime light (NTL) data at daily scales presents an innovative foundation for monitoring human activities, offering vast potential across various research domains such as urban planning and management, disaster monitoring, and energy consumption. The VNP46A2 dataset, sourced from NPP/VIIRS, has been providing globally corrected daily NTL data since 2012. However, persistent challenges, such as fluctuations in daily NTL series due to spatial mismatch and angular effects, as well as missing data holes, have significantly impacted the accuracy and comprehensiveness of extracting daily NTL changes. To address these challenges, a dataset production framework focusing on error correction, interpolation, and validation was developed. This framework led to the creation of a high-quality daily NTL dataset from 2012 to 2024, named HDNTL, which specifically targets 653 cities with populations predictably exceeding one million in 2025. A comparative analysis with the VNP46A2 dataset revealed promising results in spatial mismatch correction for two sample areas—the airport and flyover (angular effect can be ignored). These areas exhibited reduced fluctuations in HDNTL time series and maintained or strengthened weekly periodicity, which reflects traffic flow dynamics. Furthermore, the correction of angular effects across various urban building landscapes demonstrated sound improvements, mitigating angular effects in different directions and reducing periodicity from the angular impacts. The spatiotemporal interpolation of missing data holes has high similarity with the reference data, as indicated by an R^2 of 0.98, and it increased the valid pixels of all cities by 15.12%. The HDNTL dataset exhibited enhanced consistency with high-resolution SDGSAT-1 data regarding the NTL change rate and alignment with ground truth data of power outages, showcasing superior performance in short-event detection. Overall, the HDNTL dataset effectively mitigates instability in daily series caused by spatial mismatch and angular effects observed in VNP46A2, improving data comparability across time and space dimensions. This dataset enhances the ability of the NTL to reflect the ground events, providing a more accurate reference for daily-scale nighttime light research. Additionally, the dataset production framework facilitates easy updates from future VNP46A2 products to HDNTL. The HDNTL is openly available at https://doi.org/10.5281/zenodo.14992989 (Pei et al., 2025).

https://doi.org/10.5194/essd-2025-142
Preprint. Discussion started: 7 May 2025

1 Introduction

Nighttime light (NTL) data captures artificial light emissions at night, serving as a distinctive proxy for monitoring human activities that differ significantly from daytime observations. Recent studies have demonstrated the powerful capability of NTL in characterizing various aspects of dynamic urban processes and societal activities: from mapping urban extents, estimating economic vitality and energy consumption, to evaluating housing vacancy rate, disaster and conflict impact, light pollution issues (Cao et al., 2009; Chen et al., 2015; Davies et al., 2023; Elvidge et al., 1997; Li and Zhou, 2017; McCallum et al., 2022; Wang et al., 2020; Zheng et al., 2022b; Zhou et al., 2014). These applications typically use yearly or monthly temporal resolutions of NTL, such as Operational Linescan System onboard Defense Meteorological Satellite Program satellites (DMSP) (Elvidge, 1997), which are valuable for studying long-term human activity and urban development.

The Day/Night Band (DNB), a key component of the Visible Infrared Imaging Radiometer Suite (VIIRS), is carried aboard the Suomi National Polar-orbiting Partnership (S-NPP) and Joint Polar Satellite System (JPSS) satellites. This sensor captures high-resolution global nighttime data in the visible and near-infrared (NIR) spectrum, enabling daily monitoring of nocturnal light emissions. NASA's Black Marble nighttime lights product suite (VNP46) has been providing daily NTL datasets based on VIIRS DNB records since January 2012 with a spatial resolution of 500 m and a temporal resolution of one day (Román et al., 2018; Miller et al., 2012), supporting more potential applications for short-term human activity monitoring. Despite the potential, daily NTL observations from VNP46 exhibit significant variability, influenced not only by variation from human activities (Román and Stokes, 2015) but also the external factors such as measurement errors and retrieval uncertainties (Wang et al., 2021; NASA, 2018). Among the current NASA Black Marble product suites, the VNP46A2 dataset has been daily moonlight- and atmosphere-corrected based on daily at-sensor TOA nighttime radiances (VNP46A1). However, the spatial mismatch, angular effect and missing data holes still introduce significant uncertainties in capturing rapid NTL intensity changes on daily time scales, thus limiting the accuracy of short-term human activities monitoring (Hu et al., 2024; Wang et al., 2021).

The spatial mismatch error arises when the 740m DNB view footprint misaligns with the 500m gridded output pixels, leading to brightness estimation errors (Hu et al., 2024) (Fig. 1a), thus causing instability in the daily NTL time series (Román et al., 2018) (Fig. 1b). Estimating the error using any model or formula is challenging since the discrepancy is random from day to day. To mitigate the spatial mismatch error, it has been recommended that a 3-by-3-pixel averaging window be applied (Román et al., 2018). However, this approach potentially causes a "blooming effect" where the signal in specific pixels becomes diffused.

The anisotropic behavior of artificial light emissions and observation—dependent on local landscape and satellite viewing angles—is yet to be addressed in VNP46A2. The S-NPP satellite experiences daily variations in the sensor's viewing zenith angle (VZA) over a 16-day orbital cycle (Tan et al., 2022). The DNB measures both artificial direct light (e.g., street lamps, vehicle headlight, indoor light through a window) and reflected light (Fig. 1a). Due to the diversity of built environments, surrounding buildings and trees create a blocking effect on light sources. For some top-covered light sources, such as

https://doi.org/10.5194/essd-2025-142
Preprint. Discussion started: 7 May 2025

streetlights and indoor lighting, visible changes may occur as the satellite's viewing angle changes. For example, these lights might not be observable from a nadir view but could be detected from off-nadir angles (Tan et al., 2022). Additionally, reflected light sources, in addition to being influenced by blocking effects and visible changes, are inherently anisotropic and are sensitive to surface reflectance (Barnsley et al., 1994). Collectively, these factors result in pronounced angular effects, which are directly reflected in the variability of NTL with respect to VZA (Wu and Li, 2024) (Fig. 1c). In urban area, this variability is closely tied to the complexity of the built environment, with Tan et al. (2022) identifying negative, U-shaped, and positive angular effect across different built environments. In general, the angular effect introduces uncertainties in the NTL time series, potentially leading to inaccuracies in estimating dynamic changes in ground truth conditions (Wang et al., 2021). Therefore, using angularly consistent NTL observations is essential to ensure the reliability and accuracy of NTL-based applications.

In addition, a certain number of pixels in cloud-free images from the VNP46A2 were masked as low quality or without valid pixel values. As a result, these cloud-free images exhibit small missing holes (see an example in Fig. 1d). Unlike pixels covered by actual clouds and snow, these small missing holes are spatially or temporally discontinuous. Some small missing holes inherently lack valid NTL values in the DNB, and another portion of holes are flagged as suspect VIIRS Nighttime Cloud Mask (VCM) detections and subsequently outputted as poor-quality mandatory QA flags (Wang et al., 2021). The benchmark test conducted during the Black Marble production illustrates that the accuracy of the quality mask varies depending on factors such as high albedos, atmospheric and geographic conditions (Wang et al., 2020). These holes pose challenges for subsequent applications, since we observe a higher proportion of missing data holes in areas with higher annual average NTL intensity, which often correspond to city cores (Fig. 1e). The high albedos of land surfaces and the high air pollution in urban cores may contribute to the errors in the quality mask. Therefore, it is crucial to interpolate these small missing holes to ensure the continuity of cloud-free images and enhance the practical application of NTL images in urban core areas.

https://doi.org/10.5194/essd-2025-142
Preprint. Discussion started: 7 May 2025

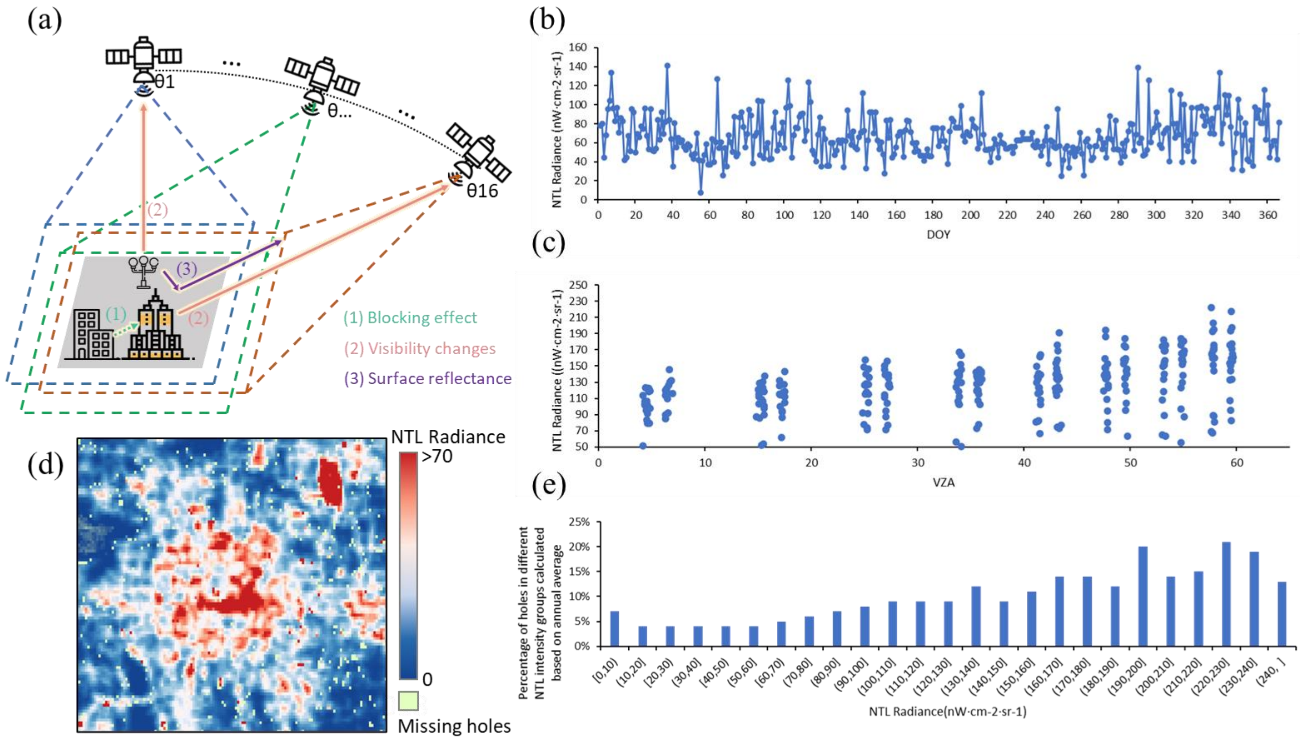

Figure 1: An illustration of spatial mismatch error, angular effect error and missing data holes of VNP46A2. (a) Schematic diagram illustrating the existence of spatial mismatch and angular effects, (b) The instability of daily NTL series, (c) The changing trend of daily NTL intensity along with VZA changes within one year, (d) Small holes existence in cloud-free NTL image of Beijing on October 1, 2018, (e) The percentage of holes in different NTL intensity groups calculated based on annual averages.

Until an effective solution is developed, researchers rely on aggregation methods, such as calculating weekly or monthly averages, to minimize the impact of uncertain errors in daily time series in regional research cases (Alahmadi et al., 2021; Zhou et al., 2022). It becomes crucial to establish a temporally consistent daily NTL dataset to conduct a quantitative analysis of human activities at finer time scales. A Self-adjusting method featuring Filter and Angular effect Correction (SFAC), proposed by Hu et al. (2024), provides an effective solution to mitigate errors arising from spatial mismatch and angular effects. The SFAC only requires the original NTL data and does not require other auxiliary data for error correction. Therefore, it has strong generalization ability and is conducive to producing a dataset. However, the issue of small missing holes remains unresolved, which leads to incomplete temporal and spatial coverage, especially in urban central areas (Fig.1e). In addition, using the annual average value as the reference for correcting the angular effect can easily mask the satellite observation angle information of the corrected data, leading to inconsistent-angle adjusted results. When combined with knowledge of the local building environment, this angle information can help users better identify the sources of light captured by the satellite.

This study aims to address these gaps by developing a refined dataset that enhances the accuracy and reliability of daily NTL observations. Such improvements are critical for facilitating more precise short-term urban dynamics and human activities analyses. To achieve this, we refined and optimized the SFAC method by adjusting the data to a consistent satellite

https://doi.org/10.5194/essd-2025-142
Preprint. Discussion started: 7 May 2025

monitoring angle and developed a spatiotemporal interpolation method to ensure the completeness of cloud-free images. Focusing on 653 major cities with populations projected to exceed 1,000,000 by 2025, our dataset targets densely populated urban centers worldwide. As population and economic activity hubs, these cities play a crucial role in shaping the nocturnal landscape visible through remote sensing. It is important to note that the framework developed in this study is versatile and can be applied to any region, including small cities, towns, and rural areas, to produce high-quality daily NTL time series. We will make the code from this study available for users who wish to generate such data beyond the 653 major cities. Our work aims to support sustainable urban development initiatives globally by delivering accurate and detailed daily NTL data.

2 Data

2.1 Study area

By 2030, one-third of the global population is projected to live in cities with over 500,000 inhabitants (United Nations, 2018). Among these, urban centers exceeding one million inhabitants are vital hubs driving global economic, cultural, technological, and social progress. These cities are at the forefront of global challenges such as climate change, energy transition and urbanization. Prioritizing the growth and sustainability of these cities is paramount for fostering global prosperity and sustainable development. To aid these urban centers with valuable NTL insights, and help their urban dynamics monitoring, our study focuses on producing a high-quality daily nighttime light dataset (HDNTL) for 653 cities with a projected population of more than 1,000,000 by 2025, based on the World Urbanization Prospects (WUP): The 2018 Revision (United Nations, 2018). The location of the 653 cities is shown in Fig. 2. The HDNTL dataset generation process is not limited by city size or location, as it relies on pixel-level processing of NTL data. To facilitate broader application, we will make our code open-source, enabling researchers and practitioners to generate HDNTL datasets for other cities of interest.

The extent of each city is adaptively determined based on the GHS Degree of Urbanisation Classification (GHS-DUC) dataset (Schiavina et al., 2021). The production process of the extent is as follows: (1) Reclassify the GHS-DUC data into urban core area ("city", "dense town", and "semi-dense town" in GHS-DUC), suburban and rural area ("suburbs or peri-urban area", "village", "dispersed rural area", and "mostly uninhabited area" in GHS-DUC), and non-land area (including oceans and inland water bodies, categorized as "not on land" in GHSL); (2) Grow a square with the central coordinates of each city until the total urban core area divided by the total suburban and rural area within the square is less than 1. This square is defined as the city's Region of Interest (ROI). Most cities' built-up areas are encompassed within the adaptive ROI. Some cities in close proximity may have overlapping ROIs, as seen in the close-up ROI of cities in the Yangtze River Delta in China, shown in Fig. 2. In addition, the United Nations utilizes urban agglomeration as a population metric, yet the provided center coordinates are for the primary city within the agglomeration, which may result in the generated adaptive boundaries not covering all cities in the urban agglomerations. To address this issue, visual inspection and manual adjustment were carried out.

https://doi.org/10.5194/essd-2025-142
Preprint. Discussion started: 7 May 2025

Open Access Earth System Science Data Discussions

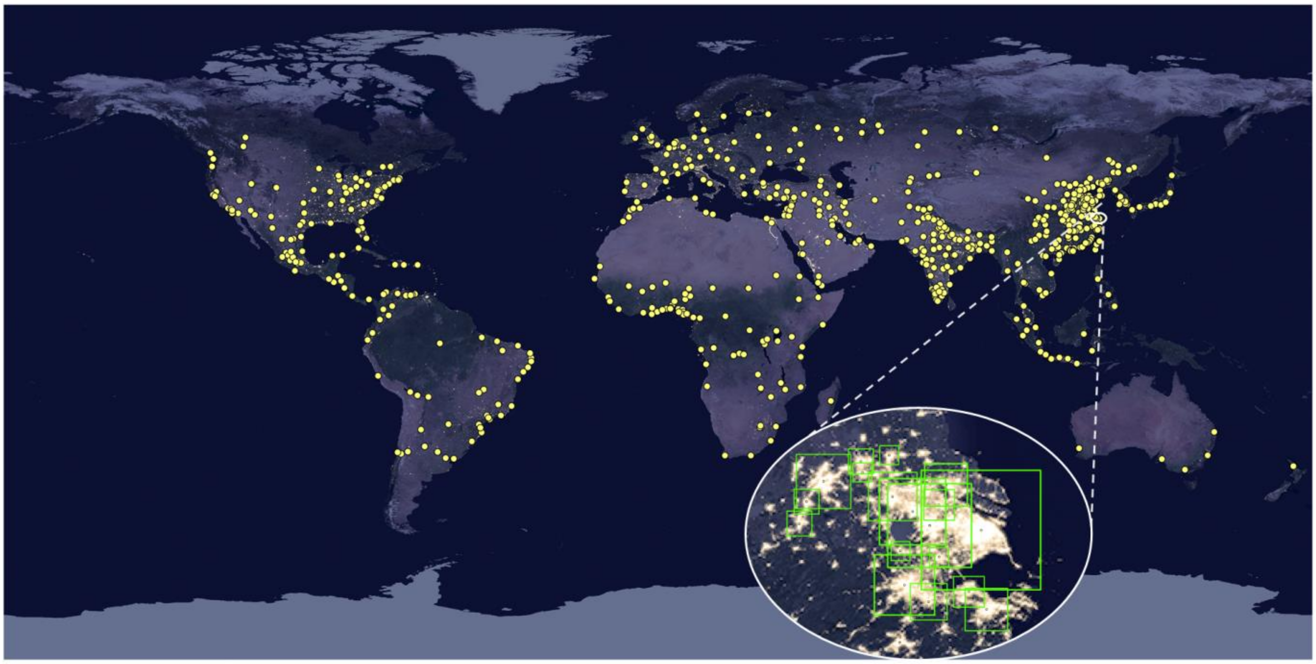

Figure 2: Location of the 653 cities included in HDNTL and a close-up of the ROIs of cities in part of the Yangtze River Delta in China. Background NTL image from NASA (https://earthobservatory.nasa.gov/features/NightLights).

2.2 Data source and preprocessing

We obtained daily VNP46A2 data from 2012 to 2024 for 653 cities, and used the "DNB_BRDF-Corrected_NTL" band as the nighttime light data to be further corrected (NASA, 2018). At the same time, the "Sensor_Zenith" band of VNP46A1 data was obtained as a reference for angular effect correction (NASA, 2012). Regarding quality control, we used the mandatory quality flag, snow cover flag, and cloud mask quality flag to screen high-quality observations.

To verify the effectiveness of the data correcting process, we compared the processed data with the unprocessed data to investigate whether the spatial mismatch problem and the angular effect problem were effectively alleviated. In addition, to verify the dataset's ability to reflect the ground artificial light changes, we collected high spatial resolution NTL datasets represented by SDGSAT-1 data and a power outage statistic report as comparative verification data. The SDGSAT-1 is equipped with a glimmer imager capable of capturing low-light nighttime data with a revisit cycle of 11 days. We computed the grayscale brightness from the RGB band (40m resolution) as a comparative reference. To avoid the spatial mismatch between the HDNTL and SDGSAT-1, we resampled both datasets to 1 km during verification. Given the high spatial resolution of SDGSAT-1 data, we have grounds to believe that the resampled SDGSAT-1 is less prone to the spatial mismatch issue observed in VNP46A2 data. Due to the limited availability and quality of SDGSAT-1 data, we only selected the SDGSAT-1 NTL images of Tianjin, China, on January 25 and February 21, 2022, for comparisons (https://www.sdgsat.ac.cn/).

NTL can directly reflect the lighting pattern of artificial lights at night, directly responding to power outages. The validity of the dataset can be evaluated by comparing the power outage response before and after data processing. On September 20,

https://doi.org/10.5194/essd-2025-142
Preprint. Discussion started: 7 May 2025

2017, Hurricane Maria landed in Puerto Rico as a Category 4 storm, becoming the most serious hurricane to affect the island since 1928. After the hurricane, there was a large-scale and long-term power shortage across the island. We obtained the Hurricanes Nate, Maria, Irma, and Harvey Situation Reports provided by the U.S Department of Energy (https://www.energy.gov/ceser/articles/hurricanes-nate-maria-irma-and-harvey-situation-reports), screened the daily reports 10 days before the hurricane and one month after the hurricane, and selected the percent of total customers without power in the report as the parameter for calculating the official power supply index.

3 Methodology

As Fig. 3 shows, we proposed a four-step framework to generate the HDNTL dataset based on VNP46A2 after data preprocessing. During preprocessing, only the highest-quality observations are retained based on the mandatory quality flag, snow cover flag, and cloud mask quality flag. The first step was to correct the spatial mismatch, the second step was to fix the angular effect, and the third step was to interpolate the small missing holes based on spatial and temporal information. Finally, a thorough dataset validation was conducted, including examining the effectiveness of spatial mismatch and angular effect corrections, interpolation accuracy, comparing results with high-resolution NTL datasets, and investigating the application capability in different events.

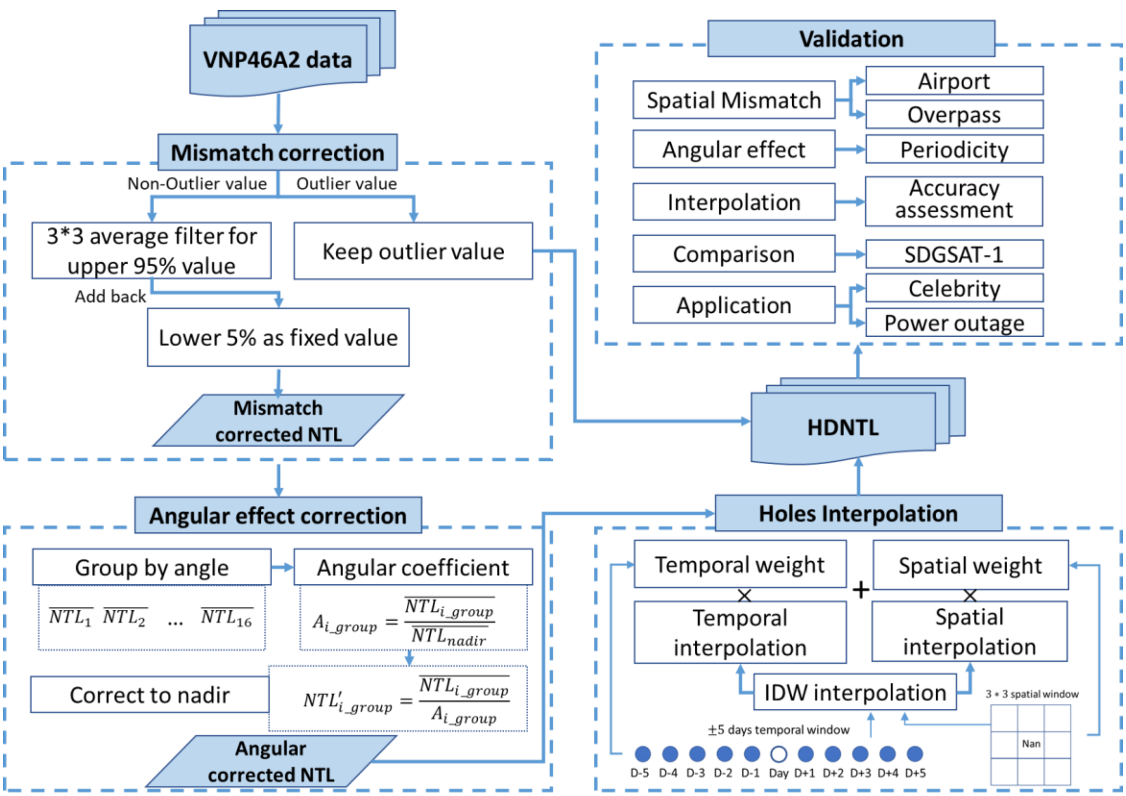

Figure 3: Flow chart of the generation of HDNTL.

https://doi.org/10.5194/essd-2025-142
Preprint. Discussion started: 7 May 2025

3.1 Spatial mismatch and angular effect correction

We referred to SFAC (Hu et al., 2024) to eliminate the spatial mismatch and angular effect. To mitigate observation variability induced by discrepancy of daily DNB view geometry, the SFAC method employs a fixed area assumption. This fixed area corresponds to the pixel's stable light signature, with the inter-daily brightness variations caused by footprint displacements being identified as the mismatch effect. The NTL is formulated in SFAC as:

$$NTL = A * \left(NTL_{fix} + NTL_{variation}\right) + NTL_{\ mismatch} + \varepsilon \ , \tag{1}$$

Where NTL_{fix} means the light from the fixed area, $NTL_{\ mismatch}$ is the light that exists at the edge of the daily changing footprint and outside the fixed area (Fig. 1a); $NTL_{variation}$ represents the changes in NTL that are extremely different from regular patterns due to specific events. A is the angular effect coefficient that helps correct NTL at different observation angles to the nadir observation. ε denotes residual random noise, which could originate from initial sources or be introduced during the product generation process.

The SFAC method employs a specialized A-average filter to address spatial mismatch effects. This approach operates under the principle that the fixed area (representing stable light emissions) is inherently smaller than the daily varying sensor footprint. Unless specific events, such as power outages or holiday celebrations, cause the NTL to suddenly weaken or strengthen, it is reasonable to assume that the annual lowest light intensity is close to the NTL_{fix}. The A-average filter processes daily NTL time series through three key steps. First, the $NTL_{variation}$ is identified and removed using a 3 times standard deviation threshold relative to the annual mean light radiance. The dates with $NTL_{variation}$ observations are marked. The NTL_{fix} is then determined as the mean of the lowest 5% NTL radiance for non-variation days. Subsequently, the $NTL_{\ mismatch} + \varepsilon$ is obtained by subtracting NTL_{fix} from NTL without $NTL_{variation}$. The SFAC applied a 3 × 3 pixel averaging filter for $NTL_{\ mismatch} + \varepsilon$, and add back NTL_{fix} to complete the correction process of spatial mismatch. For those days when extreme events occurred ($NTL_{variation}$), the SFAC chose to directly retain the original values in the final dataset, which not only preserved the event signal but also avoided the diffusion of the event signal component during the processing.

In the production process of the HDNTL dataset, we made subtle improvements to the angular effect correction in the SFAC method by shifting from an annual average-based correction approach to a nadir observation-based correction approach. This adjustment is necessary for several reasons. First, NTL images are frequently affected by clouds, snow, and atmospheric conditions, resulting in data gaps. Since angular effects have been well-documented, these missing data can lead to insufficient observations at certain angles. When using valid observations for the annual average calculation, observations at some angles may be overrepresented, while others may be underrepresented. This imbalance can introduce additional uncertainties into the angular effect correction process. Additionally, the annual average method may introduce regional biases, particularly in areas exhibiting distinct angular effect patterns (Tan et al., 2022). Since the annual average may represent different viewing angles in different regions, this inconsistency in angular observations can reduce the spatial comparability of the dataset. Such biases can undermine the reliability of the dataset for cross-regional analyses, such as comparing urbanization trends or energy

https://doi.org/10.5194/essd-2025-142
Preprint. Discussion started: 7 May 2025

consumption patterns between cities. By adopting a nadir observation-based correction approach, we can effectively mitigate these biases, ensuring more consistent and spatially comparable NTL data representation across diverse built environments.

The S-NPP satellite adopts a sun-synchronous polar orbit and completes a revisit cycle every 16 days. This orbital configuration ensures that each ground location maintains essentially the same VZA observation sequence within the 16-day cycle in a given year. Based on this characteristic, we stratified a year's daily NTL time series data into 16 distinct VZA groups. We calculated the mean NTL radiance for each group, with the near-nadir observation group (VZA < 6º) serving as the reference group for angular effect correction. The angular effect coefficients and correction value of the remaining groups were calculated as follows:

$$A_{i\_group} = \frac{\overline{NTL_{i\_group}}}{\overline{NTL_{nadir}}} \tag{2}$$

$$NTL'_{i\_group} = \frac{\overline{NTL_{i\_group}}}{A_{i\_group}} \tag{3}$$

Where $\overline{NTL_{i\_group}}$ represents the average light radiance of the $i\ th$ angular group, $\overline{NTL_{nadir}}$ is the average light radiance of the reference nadir group (VZA < 6º), A_{i_group} is the angular effect coefficient for the $i\ th$ group. NTL'_{i_group} is the angular-corrected NTL radiance for i -th group.

3.2 Spatiotemporal interpolation of small holes

Unlike conventional space or time-filling methods, spatiotemporal filling methods leverage more information and achieve higher accuracy (Hao et al., 2023; Tan and Zhu, 2023). Therefore, this study designed an efficient interpolation method that integrates spatial and temporal information to estimate pixel values of small holes. To distinguish missing value holes from those caused by extensive coverage of the cloud mask, we define the missing value hole as a missing value pixel with valid neighboring observations in the spatial windows. Considering the significant heterogeneity of urban areas, we chose the smallest spatial unit for spatial interpolation, a 3×3 window. As for time interpolation, it has been proven that for VNP46A2 data, an average of 16 days of compositing is required to ensure at least 95% effective pixel coverage of the city (Zheng et al., 2022a). Therefore, we tested the single-sided temporal window from 1 to 8 days. The temporal interpolation window was finally determined based on the evaluation of interpolation accuracy and effectiveness. The interpolation process is as follows:

$$NTL_{is} = \sum_n^N \omega_n NTL_n \tag{4}$$

$$NTL_{it} = \sum_m^M \omega_m NTL_m \tag{5}$$

$$NTL_i = a_{is} NTL_{is} + a_{it} NTL_{it} \tag{6}$$

$$a_{is} = \frac{\sum_n^N \omega_n}{\sum_n^N \omega_n + \sum_m^M \omega_m},\ a_{it} = \frac{\sum_m^M \omega_m}{\sum_n^N \omega_n + \sum_m^M \omega_m} \tag{7}$$

Where NTL_{is} is the spatial fill value for pixel i, n is the n-th pixel in a 3×3 window centered on pixel i, ω_n is the inverse distance spatial weight of pixel n, NTL_n is the NTL of pixel n; NTL_{it} is the temporal fill value for pixel i, m is the m-th day in the temporal window centered on the target date for pixel i, ω_m is the inverse distance temporal weight of pixel m, NTL_m is the NTL of pixel i at day m; NTL_i is the spatial-temporal interpolated NTL for pixel i, a_{is} is the relatively spatial weight,

a_{it} is the relatively temporal weight. The above interpolation process was conducted for data after spatial mismatch and angular effect corrections and only applied to missing pixels with valid neighboring observations in the spatial and temporal windows. $NTL_{variation}$ is also excluded during interpolation and added back after interpolation. We do not interpolate missing pixels caused by large and long-persistent clouds because the interpolation is unreliable (Román et al., 2018).

3.3 Validation strategy

3.3.1 Spatial mismatch and angular effect correction

Spatial mismatch errors can cause large fluctuations in the time series of NTL data. Therefore, the effectiveness of spatial mismatch correction can be evaluated by investigating the daily NTL data of regions with relatively stable lights. In addition, to eliminate the superposition effect of angular effect correction, we selected airports and flyovers as sample sites to conduct this evaluation for the following reasons: (1) As functional areas with transportation attributes, airports and flyovers generally do not experience large fluctuations in daily light changes, are less affected by extreme events, and tend to be more stable in time series. (2) Airports are generally built in open areas, and flyovers are generally built several meters above the ground. The building density around both sites is low, so they are less affected by angular effects.

Since periodic VZA induces observed periodicity of daily NTL series (Tan et al., 2022), the periodic weakening of the NTL with VZA changes can prove the effective correction of the angular effect. To assess the periodicity, we employed the periodic basis vectors following the approach of Liu et al. (2019). Given the 16-day periodicity of VZA, 16 orthogonal vectors ei $(i = 1, \ldots, 16)$ were established, each representing distinct VZA variations. The time series data were projected onto these orthogonal vectors using principal component analysis. The periodicity for each day within the cycle $(i = 1, \ldots, 16)$ was quantified by computing the ratio between the projection vector's norm and the NTL radiance time series vector's norm, expressed as the Information Rate (IR) (Jia et al., 2023). The higher the IR, the higher the periodicity of the 16-day cycle. The overall periodicity $(i = 1, \ldots, 16)$ was determined by aggregating all individual periodicities:

$$IR_i = \sum_{j=1}^{n} IR_i^j \tag{8}$$

Where IR_i is the IR of a pixel i. IR_i^j is the IR of pixel i of $j\ th$ day in the cycle. n is the length of the cycle. To gain a regional evaluation, we calculated the average value of IR_i of all pixels (total number = N) inside a given region as an assessment metric, the equation is:

$$IR^{region} = \frac{1}{N} \sum_{i=1}^{N} IR_i \tag{9}$$

3.3.2 Spatiotemporal interpolation of small holes

To evaluate the accuracy and reliability of the spatiotemporal interpolation method and determine the optimal temporal window size, we designed a comprehensive validation approach that considers both interpolation accuracy and the availability of valid reference data within the interpolation window. We selected 300 images randomly from the dataset that had already

https://doi.org/10.5194/essd-2025-142
Preprint. Discussion started: 7 May 2025

undergone spatial mismatch and angular effect corrections. In each image, we randomly masked out a subset of high-quality pixels with at least one valid value in a 3×3 spatial window, treating them as "small missing holes". The original values of these masked pixels were retained as reference data for comparison. Single-sided temporal windows were tested from 1 to 8 days to evaluate the impact of window size on interpolation accuracy, and the interpolated values were compared with the reference values using R^2, RMSE, and MAE as evaluation metrics. Additionally, we assessed the relative temporal weight for each window size, with higher weights indicating a greater proportion of valid reference data and higher reliability.

3.3.3 Short-period event detection

The corrected NTL time series should have eliminated false fluctuations to improve the monitoring sensitivity of specific events, especially the response to sudden weakening or strengthening. We selected two cases for analysis. The first case refers to the 2023 Liuyang Fireworks Festival (LFC) held in Liuyang City, Hunan Province, China, on the evening of November 4, 2023. After a four-year hiatus due to COVID-19, the festival scale was grand, with tens of thousands of fireworks set off at 49 points in the main urban area of Liuyang. The fireworks festival also presented a variety of themed activities and night markets, attracting a large number of citizens and tourists. The event lasted until the early morning of November 5. During this period, the light intensity in this area should be significantly enhanced compared with regular dates. The second case is the Beirut Port explosion on August 4, 2020, resulting in a death toll of at least 220 people, with over 7,000 injured and 60 people reported missing. In the affected area centered on the explosion site, a large area of buildings was damaged, and power outages occurred, leaving 300,000 people homeless. During this period, the area should have lower light intensity than usual. For the above two cases, we used the detectability index (DA) to detect whether the NTL value on the day of the event was consistent with expectations (Hu et al., 2024). We compared the detection advantage of HDNTL over the VNP46A2 dataset. When the absolute value of DA is greater than 3, it means that the value of this event deviates statistically significantly from the normal distribution and may be an outlier or extreme value. The DA is calculated as follows:

$$DA = \frac{NTL_{event} - NTL_{mean}}{NTL_{StdDev}} \tag{10}$$

Where NTL_{event} is the NTL intensity for a pixel on the event day, NTL_{mean} represents the average NTL intensity for a pixel over a given year, NTL_{StdDev} denotes the standard deviation of NTL intensity for a pixel over a given year.

3.3.4 Estimation of power outage and restoration

In addition to assessing the ability to monitor short-term events, we also focus on whether the corrected NTL data can more accurately reflect the actual situation on the ground. Artificial light creates the NTL landscape, and power outages are directly related to the reduction of NTL. Thus, the NTL data's ability to reflect the actual situation on the ground can be evaluated by comparing NTL changes and the statistics of power outages. We chose the power outage event in Puerto Rico, which was affected by Hurricane Maria. We collected daily power reports 10 days before and 1 month after the hurricane. The power

https://doi.org/10.5194/essd-2025-142
Preprint. Discussion started: 7 May 2025

supply rate is calculated as $1 - the\ percentage\ of\ affected\ customers$ in the report. To enhance the comparability of NTL data and power data reports, we designed a Customer-based Power Supply Index (CPSI) based on NTL data as below:

$$CPSI_t = \frac{NTL_t}{NTL_{pre-outage}} \times PD \tag{11}$$

Where the NTL_t represents the NTL radiance at time t, $NTL_{pre-outage}$ is the mean NTL value before the outage event in one week. PD is the percentage of the pixel-level population in the region-level population calculated based on the GHS-POP R2015A dataset (European Commission, Joint Research Centre (JRC), 2015). This index is calculated on the pixel level, and the total sum of $CPSI$ of each pixel will be the estimation of the outage situation for the whole region. It should be noted that, in order to conduct a holistic assessment of Puerto Rico, we used the HDNTL data production framework to generate data for the entire area of Puerto Rico, which is inconsistent with the ROI range in the current HDNTL dataset.

4 Results

4.1 Effectiveness of spatial mismatch correction

We used two landscapes, airports and flyovers, with less-angular effects, to demonstrate the effectiveness of spatial mismatch correction. Figure 4 shows three airport cases. The role of spatial mismatch correction is to reduce the data fluctuations caused by capturing the light sources of surrounding adjacent pixels due to different daily footprints. We used the normalized standard deviation (n-std) to see the annual fluctuation for each pixel in the case area. The first case is Beijing International Airport in 2023. A comparison of the n-std spatial distributions between VNP46A2 and HDNTL indicates that HDNTL consistently demonstrates reduced pixel-level variability in the airport region. We selected one terminal building pixel to see the annual time series, and the n-std of the NTL time series was reduced from 0.2 to 0.18, while the average did not change much. The second case is at the Los Angeles International Airport in 2023. The n-std distribution image also showed a large reduction after correction. The fluctuation of the annual time series of the selected pixel (airport runway) decreased, and the n-std reduced from 0.27 to 0.22. We can also see that the average NTL radiance of the chosen pixel increased from 38 nW·cm-2·sr-1 to 54 nW·cm-2·sr-1, which reflects that, due to the existence of spatial mismatch, the NTL is significantly underestimated due to the footprint of no obvious lights outside the runway. The third case is Sydney Airport in 2023. We also chose the runway pixel. The runway of Sydney Airport is built on the sea, so it should have lower lights. However, the VNP46A2 was overestimated due to the spatial mismatch. After correction, the NTL decreased, and n-std decreased from 0.23 to 0.17.

https://doi.org/10.5194/essd-2025-142
Preprint. Discussion started: 7 May 2025

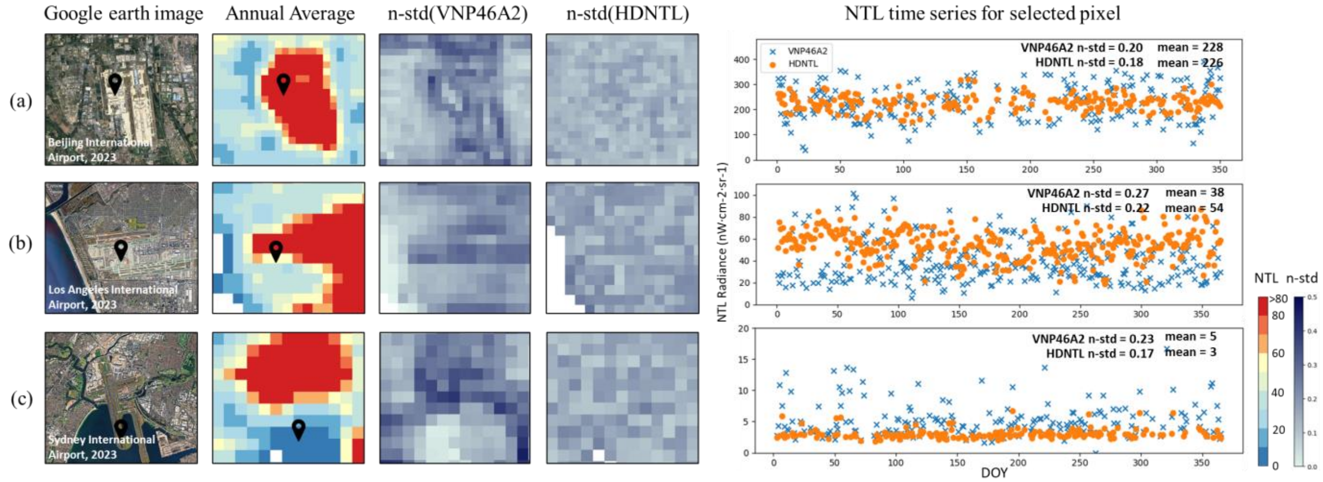

Figure 4: Spatial mismatch correction effectiveness in less-angular effect area within airport cases. (a) Beijing International Airport, (b) Los Angeles International Airport, (c) Sydney International Airport. Google Earth images © 2025 Google LLC.

Flyover is another site less affected by the angular effect, which could be a good sample to validate the effectiveness of spatial mismatch correction. Taking the Xizhimen Flyover in Beijing as an example, its three-layer structure design makes the bridge deck high, and the blocking effect of surrounding buildings is small (Fig. 5a). From the time series at the center pixel of the flyover, the HDNTL time series in 2021 showed significant improvement (Fig. 5d). Firstly, the n-std reduced from 0.22 to 0.18, which means the daily instability of the data significantly decreased. Secondly, as urban transportation infrastructure, the light source of the flyover includes not only street lights but also car lights. Therefore, the NTL radiation values can reflect the changes in traffic flow (Chang et al., 2019). We grouped the time series of the targeted year from Monday to Sunday (Fig. 5b and 5c) and drew a line chart of the average value of each group. We also calculated the IR by changing the periodicity to 7. The VNP46A2 data showed the NTL was higher from Friday to Monday, and lower from Tuesday to Thursday, and the IR for a weekly periodicity is 0.993 (Fig. 5b). After data processing, we found that the instability of the data has been reduced, with the n-std reduced from 0.22 to 0.18, while the periodicity of the data has been retained and even enhanced, with the IR increased to 0.998. We also found a higher NTL radiance from Friday to Monday, and a lower NTL radiance from Tuesday to Thursday in HDNTL (Fig. 5c). From the above cases, we can see that the correction effect for the spatial mismatch is evident, which does not only enhance the stability of the NTL time series, but also maintains the periodicity of the NTL time series, which is effective and undistorted.

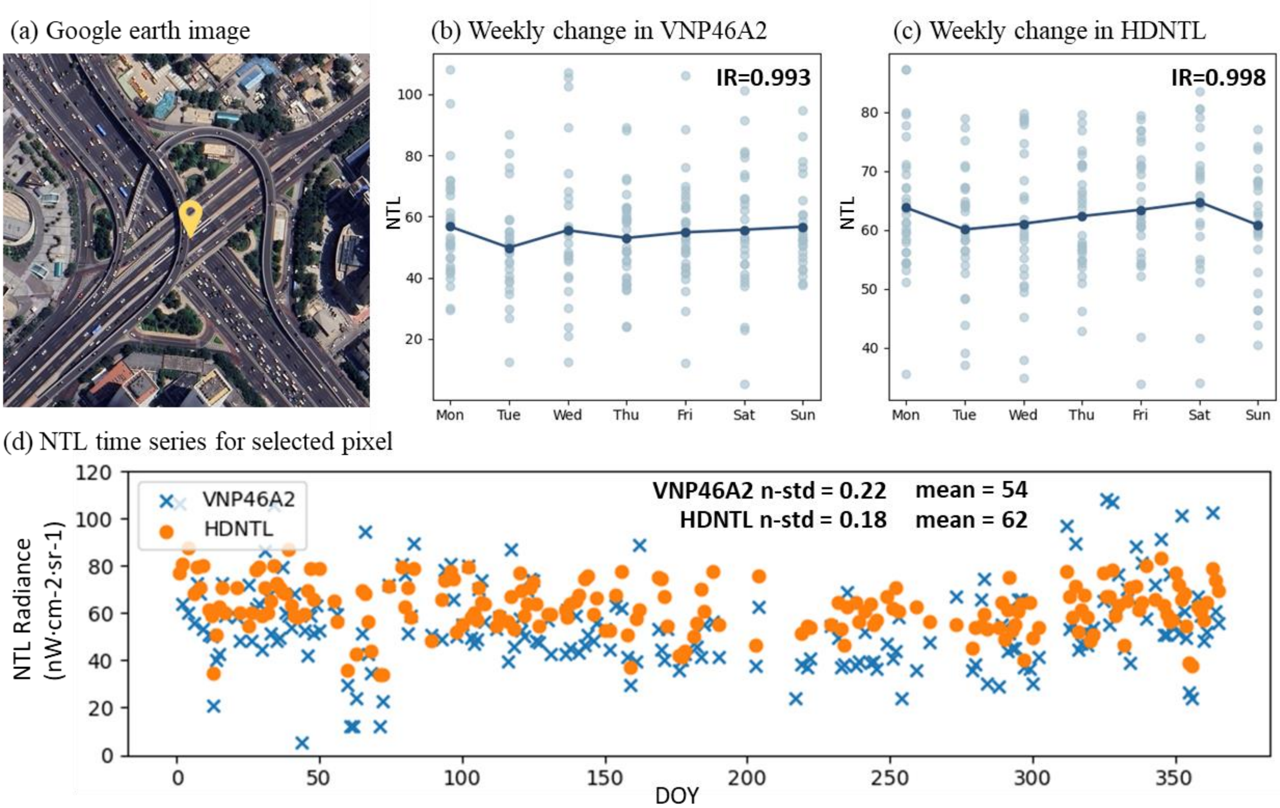

Figure 5: Spatial mismatch correction effectiveness in the less-angular effect area within the flyover case in Beijing. Google Earth image © 2025 Google LLC.

4.2 Effectiveness of angular effect correction

Previous literature has proved that the angular effect is highly correlated with the surface built-up landscape (Tan et al., 2022, 2023). When VZA changes, the blocking effect and visibility changes may lead to the angular effects in different directions. Specifically, areas with dense and high buildings, such as urban core areas, tend to have a negative angular effect, that is, NTL decreases with increasing VZA. A U-shaped angular effect tends to be produced in the transition area between urban core areas and suburban bungalows. Suburban areas where bungalows are the main buildings tend to have a positive angular effect because the blocking effect is reduced. We selected three representative areas from 653 cities with different surface built-up landscapes to explore whether the IR related to the angular effect was significantly reduced after data correction.

For the first case, we selected part of the core area of Tokyo. The Google Earth 3D map (Fig. 6a) shows many high-rise buildings here with a high density. We drew the NTL series of one pixel of this region in 2021. Due to the blocking effect of high-rise buildings, the changing trend of NTL with the increase of VZA was consistent with the negative angular effect. After correction, this trend was no longer apparent, and the IR showed that the periodicity caused by the angular effect after treatment

https://doi.org/10.5194/essd-2025-142
Preprint. Discussion started: 7 May 2025

was reduced from 0.390 to 0.138, with a reduction rate of 64.62%. The second case is a residential and industrial area near the core area of Sao Paulo, Brazil, with a relatively complex building structure. From the NTL time series of one pixel, the area here had an apparent U-shaped angular effect, that is, with the increase of VZA, NTL first decreased and then increased. After correction, this trend was also significantly weakened, and the periodicity of IR was reduced from 0.398 to 0.141, with a reduction rate of 64.57%. The third scenario pertains to Toronto, Canada, focusing on a residential locality far from the city center. The buildings here predominantly feature flat and low-rise buildings. It can be seen that the NTL series before treatment had a significant increase trend with the increase of VZA, which was a positive angular effect. After correction, this trend was also weakened, and IR was reduced from 0.382 to 0.129, with a reduction rate of 66.77%. In general, HDNTL can perform effective angular effect correction for different urban built environments, greatly enhancing the comparability of data in different spaces and times.

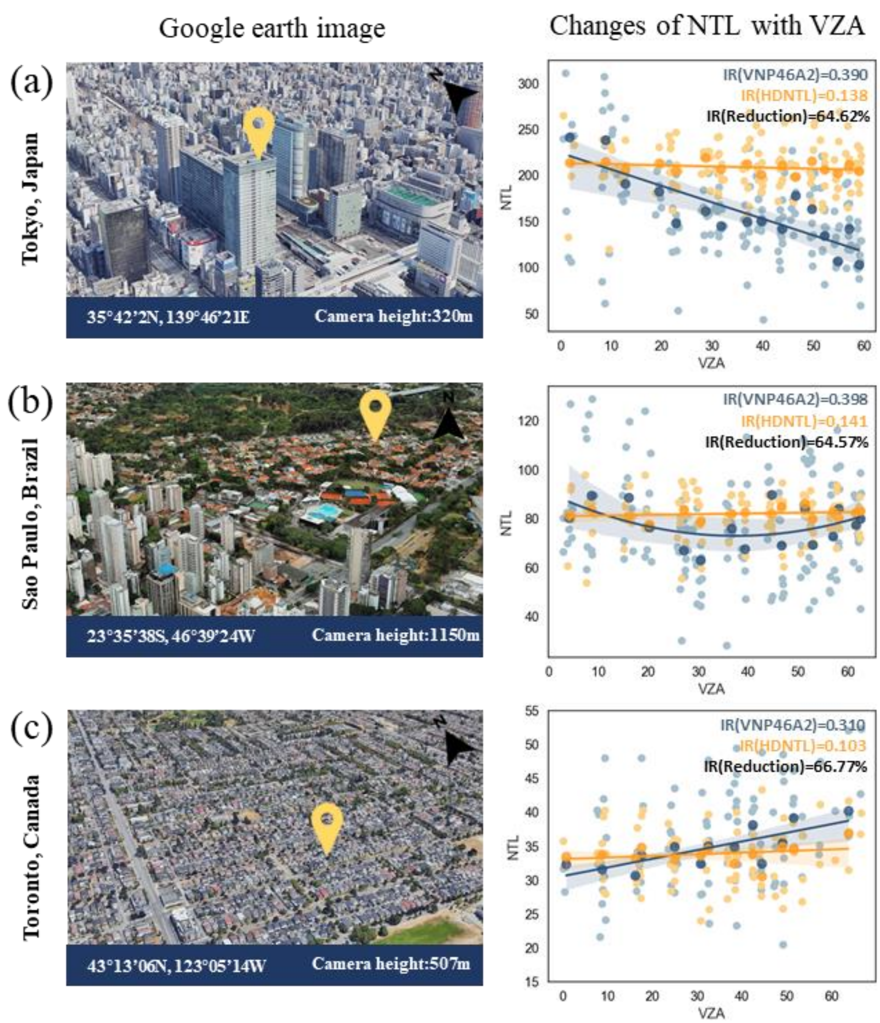

Figure 6: Angular effect and its correction effectiveness in different built-up environments. Google Earth images © 2025 Google LLC.

https://doi.org/10.5194/essd-2025-142
Preprint. Discussion started: 7 May 2025

4.3 Effectiveness of small holes interpolation

The urban surface environment presents highly heterogeneous characteristics due to the transformation and intervention of human activities. Therefore, we chose the smallest spatial window, a 3×3 window, to perform spatial interpolation of NTL, which can ensure the reliability of the interpolation results. In terms of temporal interpolation, we started with a single-sided window of 1 and gradually tested and verified the interpolation accuracy until 8. According to Fig. 7a, when the single-sided window was set to 3 and 5, the RMSE and MAE of the interpolation were lower. Further, according to Fig. 7b, when the single-sided window was 5, the relative time weight was higher, which means more valid reference values can be obtained in the time dimension. After the single-sided window was greater than 5, the marginal effect of increasing the relative time weight was weakened. Therefore, we finally chose a single-sided window of 5 for temporal interpolation. Taking into account the effective value information of time and space, we determined the relative weights of the spatial interpolation results and the temporal interpolation results, and then performed comprehensive interpolation (Eq. (6)&(7)). We randomly masked out some valid pixels for evaluating the interpolation method, i.e., interpolating these masked-out pixels, and compared the results with their original values (i.e., reference values). As shown in Fig. 7c, the linear regression R^2 between the reference value and the interpolation value was 0.98, the RMSE was 2.76, and the MAE was 1.29, indicating the high accuracy and reliability of the comprehensive interpolation method. After the hole interpolation implementation, all cities' valid pixels increased by 15.12%.

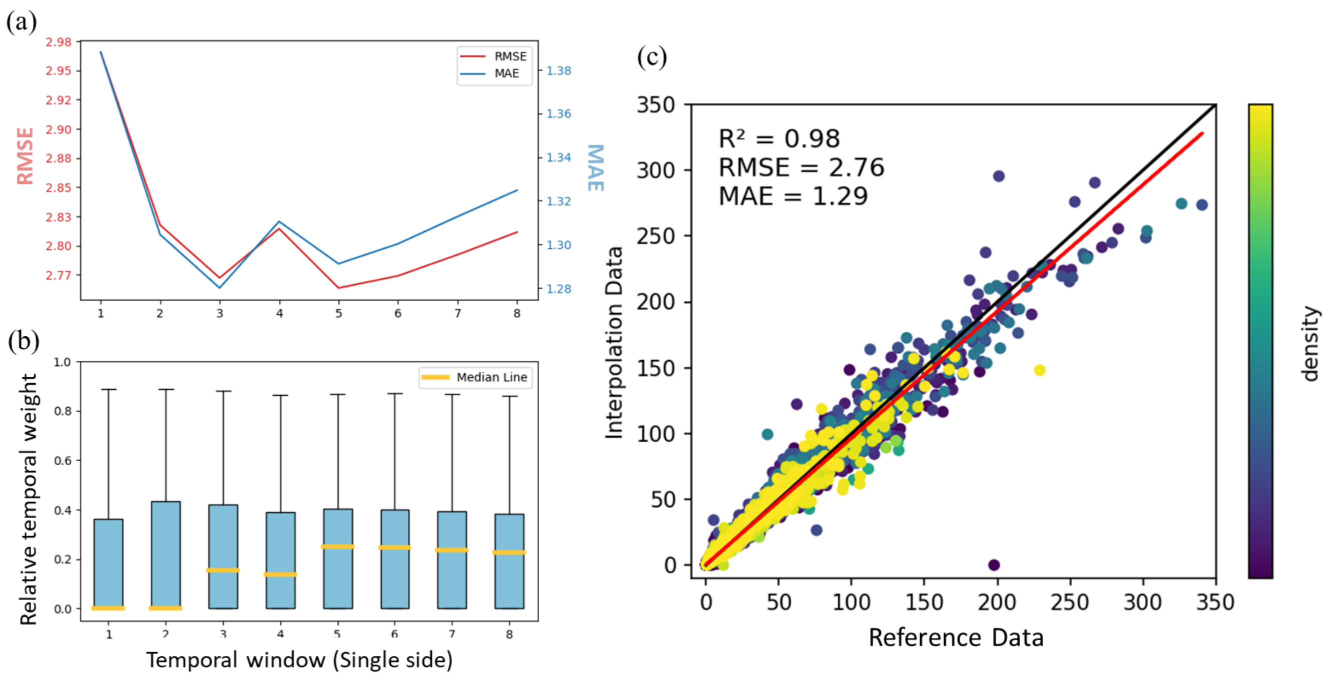

Figure 7: Interpolation accuracy test. (a) The RMSE and MAE of interpolation by different time windows, (b) The relative temporal weight of different time windows, (c) The comparison between reference data and its interpolation by the 5-day temporal window.

https://doi.org/10.5194/essd-2025-142
Preprint. Discussion started: 7 May 2025

5 Discussion

5.1 Comparison with high spatial resolution NTL data regarding temporal changes

We selected high-quality and clear nighttime light observation images from SDGSAT-1 of Tianjin on January 25, 2022, and February 21, 2022. We compared their temporal changes on pixel-level with those retrieved from HDNTL and VNP46A2. Since SDGSAT-1 is high spatial resolution data, it can be concluded that after upscaling, SDGSAT-1 is less affected by mismatch issues. Thus, the change between two SDGSAT-1 images can more accurately capture the ground light changes. The advantage of the HDNTL dataset is that it restores the daily variation characteristics of NTL, so it is expected that changes retrieved from HDNTL should be closer to SDGSAT-1. As shown in Fig. 8, the box plots of the change rate between the two days of HDNTL and SDGSAT-1 are closer, showing a consistent change trend. The VNP46A2 data show a large fluctuation in the change rate. This phenomenon reflects the significant fluctuation of VNP46A2 on the daily scale, making it challenging to capture the true characteristics of daily changes accurately. Therefore, HDNTL data appear more stable and reliable in representing NTL daily changes.

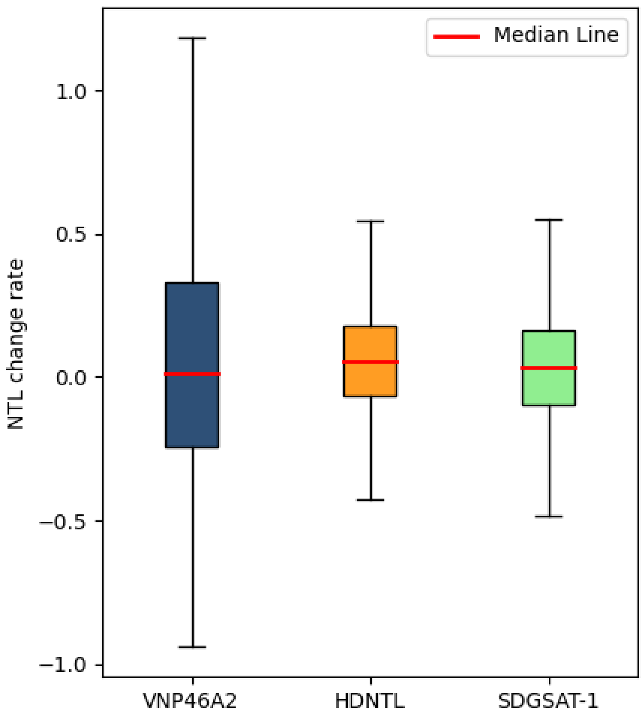

Figure 8: Comparison of temporal changing rate between SDGSAT-1, VNP46A2, and HDNTL.

5.2 Event detection regarding short-period changes

Figure 9 shows the daily NTL series of selected pixels of two short-term events in their targeted year. Figure 9a shows the daily time series of NTL for one pixel at the 2023 Liuyang Fireworks Festival (LFC) site. On the event day, the DA value

https://doi.org/10.5194/essd-2025-142
Preprint. Discussion started: 7 May 2025

calculated based on VNP46A2 was 2.1, and the DA value calculated based on HDNTL was 4.12. The absolute DA value from HDNTL was greater than 3, exceeding the mutation signal recognition threshold. For the case of a sudden drop in light, as shown in Fig. 9b, the figure shows the daily time series of NTL for one pixel at the explosion center. Before processing, the DA on the event day was -1.76, which failed to become a mutation signal. After processing, the DA was -3.63, and its absolute value was greater than 3, which can be identified as a mutation signal. This proves that after processing with spatial mismatch correction and angular effect correction, the HDNTL dataset can reduce the fluctuation of non-real situations compared to the VNP46A2 dataset, and highlight the changes in light density caused by the mutation event.

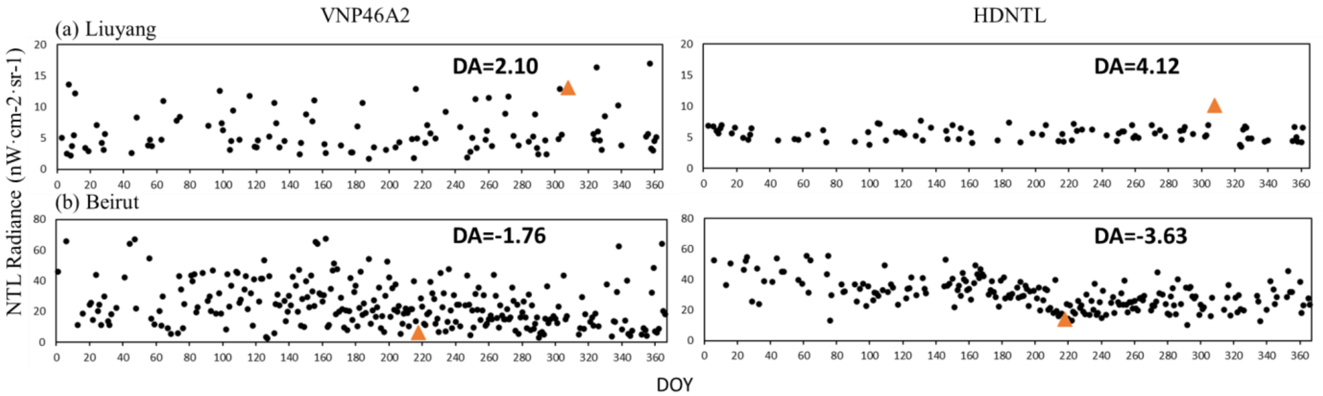

Figure 9: Two cases for short-period event detection by NTL.

5.3 Comparison with an official report regarding the power outage

According to Eq. (11), we evaluated the CPSI as the power supply index based on NTL and population density data. In this process, we chose the "Gap_Filled_DNB_BRDF_Corrected_NTL" band in the VNP46A2 data to obtain more valid values for comparison. Figure 10 shows the results of the power supply assessment using HDNTL and VNP46A2, respectively. Also, it presents the regression R^2 between the time series of the two assessment results and the official report data. The results show that the assessment results of HDNTL were more consistent with the official report, with an R^2 value of up to 0.839, which was 170% greater than the VNP46A2 data. This result emphasizes the advantages of HDNTL in capturing changes in electricity supply and further verifies the application potential of HDNTL in urban energy and disaster impact research.

https://doi.org/10.5194/essd-2025-142
Preprint. Discussion started: 7 May 2025

Open Access Earth System Science Data Discussions

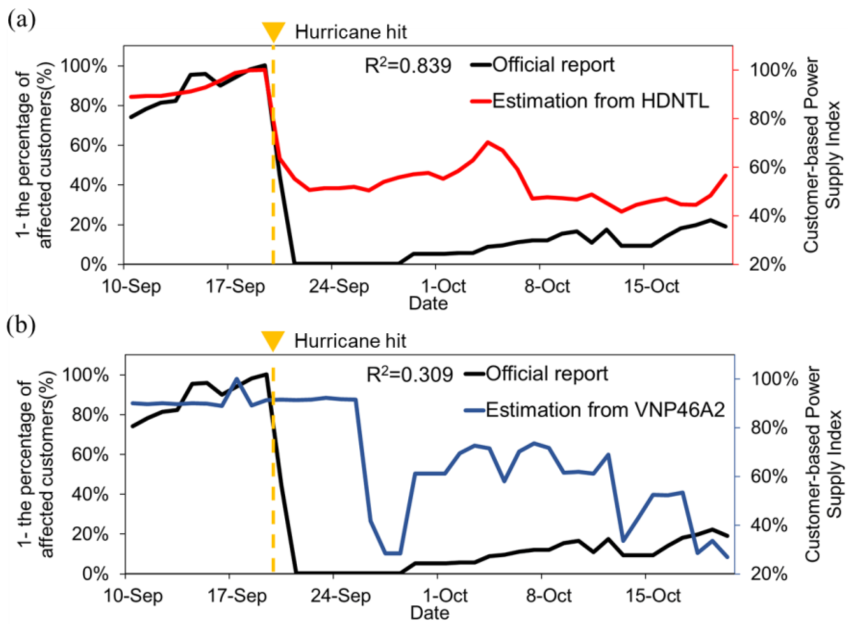

Figure 10: Comparison of CPSI calculated based on VNP46A2 and HDNTL with official report data.

5.4 Limitations

We have further improved the angular effect correction in the SFAC algorithm. In the original algorithm, the angular effect correction was based on the annual average NTL value, which would lead to some uncertainty. That is, this average value may correspond to any VZA. Existing research and the cases we discussed show that the angular effect highly correlates with the urban built environment landscape. Therefore, NTL data corrected to the same observation angle facilitate comparability between different study areas. By correcting all the data to nadir observation, theoretically, in areas with high building density and height, the NTL observation value of the nadir angle is relatively high compared with other angles. Conversely, the nadir NTL observation value is relatively low in areas with low buildings compared with other angles. Figure 11 illustrates a case in Los Angeles. Figure 11a and Fig. 11b show the corrected results based on the annual average (SFAC) and the corrected results based on nadir observation (HDNTL), respectively, both depicting the average NTL images for Los Angeles in 2024. Figure 11c displays the difference between HDNTL and SFAC. The results reveal that HDNTL data exhibits higher corrected NTL values in urban centers, particularly in areas with high-rise buildings, such as downtown Los Angeles shown in Fig. 11d. In contrast, in areas with low-rise and sparsely distributed buildings, such as the city of industry in Los Angeles shown in Fig. 11e, which features warehouses, retail stores, and car dealerships, the HDNTL data shows lower corrected NTL values. As a result, this adjustment could accentuate differences between a city's core and periphery. The HDNTL may not fully capture the facade lighting of the building, especially in low-rise building areas. Users can customize the correction parameters of the angular effect through our open-source code according to the purpose of the research.

https://doi.org/10.5194/essd-2025-142
Preprint. Discussion started: 7 May 2025

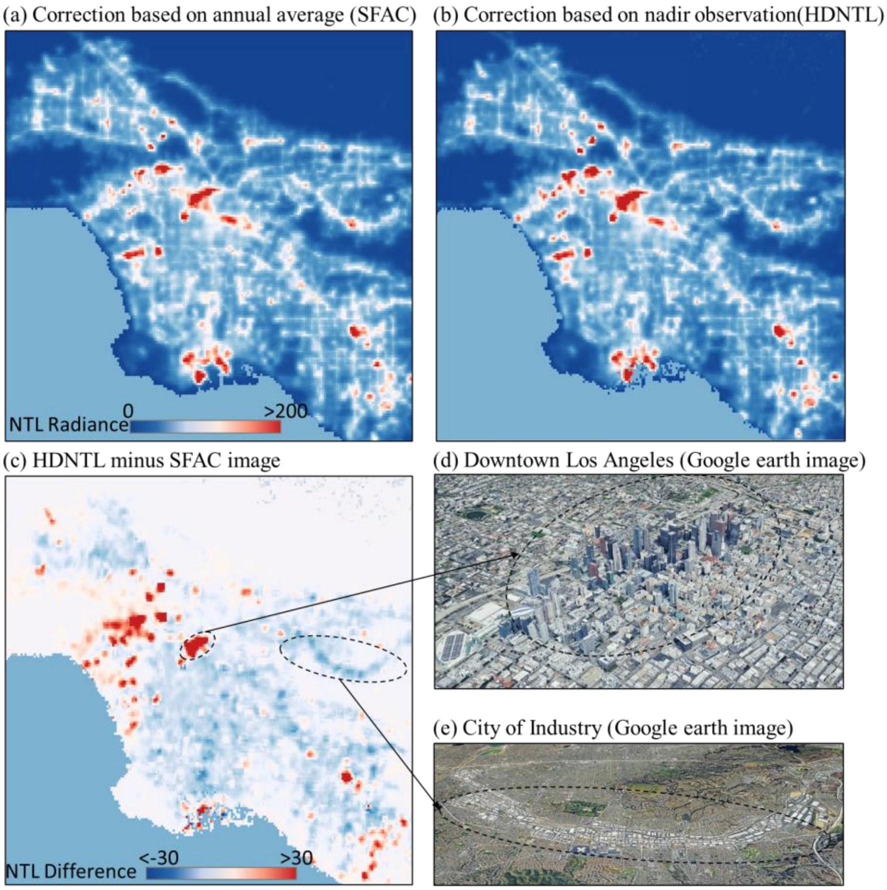

Figure 11 Comparison of angular correction results based on nadir correction (HDNTL) and annual mean correction (SFAC). Google Earth image © 2025 Google LLC.

6 Data availability

The HDNTL dataset for 653 cities from 2012 to 2024, with a spatial resolution of 15 arc-seconds (approximately 500 meters), is freely available at https://doi.org/10.5281/zenodo.14992989 (Pei et al., 2025). The data is organized in descending order of city population, with every 10 cities stored in a zip archive. City order numbers can be referenced in the data table provided in the xls format. After extraction, each city's data is stored in a separate folder, containing 13 annual NTL data in GeoTIFF format. Daily data is stored as bands within each annual NTL image.

7 Conclusion

A high-quality daily nighttime light (HDNTL) dataset for the global 653 cities (2012-2024) was produced in this study. From correction to validation, this study includes four parts: the correction of spatial mismatch, the correction of angular effect,

https://doi.org/10.5194/essd-2025-142
Preprint. Discussion started: 7 May 2025

the interpolation for small missing holes, and the validation and application. Compared to VNP46A2, in the two sample areas, airport and flyover showed a good effect on spatial mismatch correction, with a decreased n-std in annual NTL time series and maintaining or even strengthening the weekly periodicity, which reflects the traffic flow. The angular effect correction works well on three different urban building landscapes, weakening the angular effect in different directions and decreasing the angular effect's periodicity. The spatiotemporal interpolation accuracy also showed promising results in the 5+5 temporal window and 3×3 spatial window. The spatiotemporal interpolation of missing data holes is highly similar to that of reference data, as indicated by an R^2 of 0.98. After the hole interpolation implementation, all cities' valid pixels increased by 15.12%. Finally, the HDNTL showed better consistency with SDGSAT-1 data in terms of NTL change rate, and better performance in short-period event detection and alignment with power outage report data than VNP46A2. Generally, our HDNTL dataset can effectively decrease the instability of the daily NTL series caused by spatial and temporal errors in the VNP46A2, enhance the comparability of the data over different time and space, and improve the ability and accuracy of the NTL to reflect the actual events on the ground. Leveraging the degree of urbanization metrics, we have defined Regions of Interest (ROIs) for over 600 cities globally. The HDNTL dataset from 2012 to 2024 has been provided within these delineated areas. This dataset offers a valuable resource for enhanced analysis and assessment of nighttime human activity dynamics on a daily scale during the progression of urbanization.

Author contributions

ZP designed and developed the methodology, performed analysis and validation, produced the dataset, and wrote the paper. XZ supported and designed the study and wrote the paper. YH designed and developed the methodology and reviewed the paper. JC developed the methodology and reviewed the paper. XT developed the validation and reviewed the paper.

Competing interests

The authors declare that they have no conflict of interest.

Acknowledgments

This study was supported by the Research Grants Council of Hong Kong (project No.15229222), the National Natural Science Foundation of China (No. 42401474), and the Hong Kong Polytechnic University (project No. Q-CDBP).

https://doi.org/10.5194/essd-2025-142
Preprint. Discussion started: 7 May 2025

References

Alahmadi, M., Mansour, S., Dasgupta, N., Abulibdeh, A., Atkinson, P. M., and Martin, D. J.: Using Daily Nighttime Lights to Monitor Spatiotemporal Patterns of Human Lifestyle under COVID-19: The Case of Saudi Arabia, Remote Sens., 13, 4633, https://doi.org/10.3390/rs13224633, 2021.

Barnsley, M. J., Strahler, A. H., Morris, K. P., and Muller, J.: Sampling the surface bidirectional reflectance distribution function (BRDF): 1. Evaluation of current and future satellite sensors, Remote Sens. Rev., 8, 271–311, https://doi.org/10.1080/02757259409532205, 1994.

Cao, X., Chen, J., Imura, H., and Higashi, O.: A SVM-based method to extract urban areas from DMSP-OLS and SPOT VGT data, Remote Sens. Environ., 113, 2205–2209, https://doi.org/10.1016/j.rse.2009.06.001, 2009.

Chang, Y., Wang, S., Zhou, Y., Wang, L., and Wang, F.: A Novel Method of Evaluating Highway Traffic Prosperity Based on Nighttime Light Remote Sensing, Remote Sens., 12, 102, https://doi.org/10.3390/rs12010102, 2019.

Chen, Z., Yu, B., Hu, Y., Huang, C., Shi, K., and Wu, J.: Estimating House Vacancy Rate in Metropolitan Areas Using NPP-VIIRS Nighttime Light Composite Data, IEEE J. Sel. Top. Appl. Earth Obs. Remote Sens., 8, 2188–2197, https://doi.org/10.1109/JSTARS.2015.2418201, 2015.

Davies, T. W., Levy, O., Tidau, S., De Barros Marangoni, L. F., Wiedenmann, J., D'Angelo, C., and Smyth, T.: Global disruption of coral broadcast spawning associated with artificial light at night, Nat. Commun., 14, 2511, https://doi.org/10.1038/s41467-023-38070-y, 2023.

Elvidge, C. D.: Mapping City Lights With Nighttime Data from the DMSP Operational Linescan System, Photogramm. Eng. Remote Sens., 63, 727–734, 1997.

Elvidge, C. D., Baugh, K. E., Kihn, E. A., Kroehl, H. W., Davis, E. R., and Davis, C. W.: Relation between satellite observed visible-near infrared emissions, population, economic activity and electric power consumption, Int. J. Remote Sens., 18, 1373–1379, https://doi.org/10.1080/014311697218485, 1997.

European Commission, Joint Research Centre (JRC): GHS-POP R2015A - GHS population grid, derived from GPW4, multitemporal (1975, 1990, 2000, 2015) - OBSOLETE RELEASE, 2015.

Hao, X., Liu, J., Heiskanen, J., Maeda, E. E., Gao, S., and Li, X.: A robust gap-filling method for predicting missing observations in daily Black Marble nighttime light data, GIScience Remote Sens., 60, 2282238, https://doi.org/10.1080/15481603.2023.2282238, 2023.

Hu, Y., Zhou, X., Yamazaki, D., and Chen, J.: A self-adjusting method to generate daily consistent nighttime light data for the detection of short-term rapid human activities, Remote Sens. Environ., 304, 114077, https://doi.org/10.1016/j.rse.2024.114077, 2024.

Jia, M., Li, X., Gong, Y., Belabbes, S., and Dell'Oro, L.: Estimating natural disaster loss using improved daily night-time light data, Int. J. Appl. Earth Obs. Geoinformation, 120, 103359, https://doi.org/10.1016/j.jag.2023.103359, 2023.

Li, X. and Zhou, Y.: Urban mapping using DMSP/OLS stable night-time light: a review, Int. J. Remote Sens., 38, 6030–6046, https://doi.org/10.1080/01431161.2016.1274451, 2017.

Liu, S., Li, X., Levin, N., and Jendryke, M.: Tracing cultural festival patterns using time-series of VIIRS monthly products, Remote Sens. Lett., 10, 1172–1181, https://doi.org/10.1080/2150704X.2019.1666313, 2019.

https://doi.org/10.5194/essd-2025-142
Preprint. Discussion started: 7 May 2025

McCallum, I., Kyba, C. C. M., Bayas, J. C. L., Moltchanova, E., Cooper, M., Cuaresma, J. C., Pachauri, S., See, L., Danylo, O., Moorthy, I., Lesiv, M., Baugh, K., Elvidge, C. D., Hofer, M., and Fritz, S.: Estimating global economic well-being with unlit settlements, Nat. Commun., 13, 2459, https://doi.org/10.1038/s41467-022-30099-9, 2022.

Miller, S. D., Mills, S. P., Elvidge, C. D., Lindsey, D. T., Lee, T. F., and Hawkins, J. D.: Suomi satellite brings to light a unique frontier of nighttime environmental sensing capabilities, Proc. Natl. Acad. Sci., 109, 15706–15711, https://doi.org/10.1073/pnas.1207034109, 2012.

NASA: VNP46A1 - VIIRS/NPP Daily Gridded Day Night Band 500m Linear Lat Lon Grid Night, 2012.

NASA: VNP46A2 - VIIRS/NPP Gap-Filled Lunar BRDF-Adjusted Nighttime Lights Daily L3 Global 500 m Linear Lat Lon Grid, 2018.

Pei, Z., Zhu, X., Hu, Y., Chen, J., and Tan, X.: A high-quality daily nighttime light (HDNTL) dataset for global 600+ cities (2012-2024), Zenodo, https://doi.org/10.5281/zenodo.14992989, 2025.

Román, M. O. and Stokes, E. C.: Holidays in lights: Tracking cultural patterns in demand for energy services, Earths Future, 3, 182–205, https://doi.org/10.1002/2014EF000285, 2015.

Román, M. O., Wang, Z., Sun, Q., Kalb, V., Miller, S. D., Molthan, A., Schultz, L., Bell, J., Stokes, E. C., Pandey, B., Seto, K. C., Hall, D., Oda, T., Wolfe, R. E., Lin, G., Golpayegani, N., Devadiga, S., Davidson, C., Sarkar, S., Praderas, C., Schmaltz, J., Boller, R., Stevens, J., Ramos González, O. M., Padilla, E., Alonso, J., Detrés, Y., Armstrong, R., Miranda, I., Conte, Y., Marrero, N., MacManus, K., Esch, T., and Masuoka, E. J.: NASA's Black Marble nighttime lights product suite, Remote Sens. Environ., 210, 113–143, https://doi.org/10.1016/j.rse.2018.03.017, 2018.

Schiavina, Marcello, Melchiorri, Michele, Freire, and Sergio: GHS_STAT_DUC R2019A - GHS Degree of Urbanisation Classification (2015, 2000, 1990, 1975), R2019A., https://doi.org/10.2905/ED8E8E11-62C3-4895-A7B9-5EF851F112ED, 2021.

Tan, X. and Zhu, X.: CRYSTAL: A novel and effective method to remove clouds in daily nighttime light images by synergizing spatiotemporal information, Remote Sens. Environ., 295, 113658, https://doi.org/10.1016/j.rse.2023.113658, 2023.

Tan, X., Zhu, X., Chen, J., and Chen, R.: Modeling the direction and magnitude of angular effects in nighttime light remote sensing, Remote Sens. Environ., 269, 112834, https://doi.org/10.1016/j.rse.2021.112834, 2022.

Tan, X., Chen, R., Zhu, X., Li, X., Chen, J., Sing Wong, M., Xu, S., and Xu, Y. N.: Spatial heterogeneity of uncertainties in daily satellite nighttime light time series, Int. J. Appl. Earth Obs. Geoinformation, 123, 103484, https://doi.org/10.1016/j.jag.2023.103484, 2023.

United Nations: World Urbanization Prospects: The 2018 Revision, 2018.

Wang, Z, Shrestha, R., Román, M. O., 2020. NASA's Black Marble Nighttime Lights Product Suite Algorithm Theoretical Basis Document (ATBD). NASA Goddard Space Flight Center, Greenbelt, USA.

Wang, J., Roudini, S., Hyer, E. J., Xu, X., Zhou, M., Garcia, L. C., Reid, J. S., Peterson, D. A., and Da Silva, A. M.: Detecting nighttime fire combustion phase by hybrid application of visible and infrared radiation from Suomi NPP VIIRS, Remote Sens. Environ., 237, 111466, https://doi.org/10.1016/j.rse.2019.111466, 2020.

https://doi.org/10.5194/essd-2025-142
Preprint. Discussion started: 7 May 2025

Wang, Z., Román, M. O., Kalb, V. L., Miller, S. D., Zhang, J., and Shrestha, R. M.: Quantifying uncertainties in nighttime light retrievals from Suomi-NPP and NOAA-20 VIIRS Day/Night Band data, Remote Sens. Environ., 263, 112557, https://doi.org/10.1016/j.rse.2021.112557, 2021.

Wu, Y. and Li, X.: Exploring the Drivers of Variations in Daily Nighttime Light Time Series From the Perspective of Periodic Factors, IEEE Geosci. Remote Sens. Lett., 21, 1–5, https://doi.org/10.1109/LGRS.2024.3358856, 2024.

Zheng, Q., Weng, Q., Zhou, Y., and Dong, B.: Impact of temporal compositing on nighttime light data and its applications, Remote Sens. Environ., 274, 113016, https://doi.org/10.1016/j.rse.2022.113016, 2022a.

Zheng, Z., Wu, Z., Cao, Z., Zhang, Q., Chen, Y., Guo, G., Yang, Z., Guo, C., Wang, X., and Marinello, F.: Estimates of Power Shortages and Affected Populations during the Initial Period of the Ukrainian-Russian Conflict, Remote Sens., 14, 4793, https://doi.org/10.3390/rs14194793, 2022b.

Zhou, Y., Smith, S. J., Elvidge, C. D., Zhao, K., Thomson, A., and Imhoff, M.: A cluster-based method to map urban area from DMSP/OLS nightlights, Remote Sens. Environ., 147, 173–185, https://doi.org/10.1016/j.rse.2014.03.004, 2014.

Zhou, Y., Cui, Y., Gong, K., and Chen, Z.: Using Nighttime Lights to Model Power Recovery Pattern Following the Landfall of Typhoons in Eastern Coastal Areas of China, SSRN Electron. J., https://doi.org/10.2139/ssrn.4200140, 2022.